

Antiferromagnetic Order and Bose-Einstein Condensation in Strongly-Correlated Cold-Atom Systems: Bosonic t - J Model in the Double-CP¹ Representation

Yuki Nakano¹, Takumi Ishima², Naohiro Kobayashi², Kazuhiko Sakakibara³, Ikuo Ichinose², and Tetsuo Matsui¹

¹ *Department of Physics, Kinki University, Higashi-Osaka, 577-8502 Japan*

² *Department of Applied Physics, Nagoya Institute of Technology, Nagoya, 466-8555 Japan and*

³ *Department of Physics, Nara National College of Technology, Yamatokohriyama, 639-1080 Japan*

(Dated: March 14, 2018)

We study the three-dimensional bosonic t - J model, i.e., the t - J model of “bosonic electrons” at finite temperatures. This model describes a system of cold bosonic atoms with two species in an optical lattice. The model is derived from the Hubbard model for very large on-site repulsive interaction between bosons of same species (hard-core nature) and also strong correlations between different species. The operator $B_{x\sigma}$ for an atom at the site x with a two-component (pseudo-) spin $\sigma (= 1, 2)$ is treated as a hard-core boson operator, and represented by a composite of two slave particles; a spinon described by a CP¹ field (Schwinger boson) $z_{x\sigma}$ and a holon described by a hard-core-boson field ϕ_x as $B_{x\sigma} = \phi_x^\dagger z_{x\sigma}$. ϕ_x is then expressed by a pseudo-spin, which is, in turn, represented by another CP¹ (pseudo) spinon $w_{x\eta}$ as $\phi_x = w_{x2}^\dagger w_{x1}$. We then have a double-CP¹ representation of the model by $z_{x\sigma}$ and $w_{x\eta}$. By means of Monte Carlo simulations of this bosonic t - J model, we study its phase structure and the possible phenomena like appearance of antiferromagnetic long-range order, Bose-Einstein condensation, phase separation, etc. They should be compared with the possible experimental results of a recently studied boson-boson mixture like ⁸⁷Rb and ⁴¹K in an optical lattice.

PACS numbers: 67.85.-d, 11.15.Ha

I. INTRODUCTION

Cold atoms[1, 2] trapped in optical lattices are one of the most interesting systems in condensed matter physics. They are flexible because one can experimentally adjust their characteristics such as statistics and density of atoms, dimensionality of the system, signature and strength of interactions, etc.

Not only systems of single kind of atoms, but also systems of atoms of two species like a mixture of bosons and fermions are studied experimentally[3]. Recently, a boson-boson system of ⁸⁷Rb and ⁴¹K in a three-dimensional (3D) optical lattice has been studied to produce Bose-Einstein condensate[4]. The interactions among these atoms are also controllable[5].

A standard model of cold *bosonic* atoms with two species may be the bosonic Hubbard model. The two species of bosons may be described by a (pseudo-)spin $s = 1/2$ degrees of freedom. For very large strong repulsive interactions between atoms of *same species*, one may treat each boson as a hard-core boson (HCB). Thus, usual electrons of Hubbard model are to be replaced here by HCB with spins.

From this HCB Hubbard model, one can derive the *bosonic t-J* model as its low-energy effective model for a large on-site repulsion between the opposite spins (different species) and small hole concentrations[6, 7].

By using this bosonic t - J model, Boninsegni and Prokof'ev[8] studied the interplay of magnetic ordering of pseudo-spins and Bose-Einstein condensation (BEC)/superfluidity (SF) of bosonic atoms. By quantum Monte Carlo (MC) simulations, they studied the low-temperature (T) phase diagram of the two-dimensional

(2D) model for the case of *anisotropic spin coupling* $J_{x,y} = \alpha J_z$, $\alpha < 1$ and $J_z \equiv J < t$, and found the coexistence region of antiferromagnetic (AF) order and SF as a result of the *phase separation* (PS) of hole-free (AF) and hole-rich (SF) phases.

In the previous paper[9] we studied the bosonic t - J model with the isotropic coupling ($\alpha = 1$) in the slave-particle representation of operators for atoms. The usefulness of the slave-particle representation in various aspects has been pointed out for the original fermionic t - J model[10]. We expect that similar advantage of the slave-particle picture holds also in the bosonic t - J model[11].

In the slave-particle representation, the bosonic operator $B_{x\sigma}$ for atom at the site x and spin $\sigma = 1, 2$ is viewed as a composite of a spinon $z_{x\sigma}$ and a holon ϕ_x [9],

$$B_{x\sigma} = \phi_x^\dagger z_{x\sigma}, \quad (1.1)$$

where $z_{x\sigma}$ is the CP¹ spin field (Schwinger boson) and ϕ_x is the HCB.

In Ref.[9], we replaced these HCB operators of holons ϕ_x by the Higgs field with a definite amplitude,

$$\phi_x \rightarrow \sqrt{\delta} \exp(i\varphi_x), \quad (1.2)$$

where δ is the average density of holes (holons) $\delta = \langle \phi_x^\dagger \phi_x \rangle$ and φ_x is the phase degrees of freedom. This replacement is an approximation to ignore the fluctuation of amplitude of holons assuming their *homogeneous distribution*. By the MC simulations we have obtained a phase diagram and various correlation functions of the 3D model at finite temperatures ($T > 0$) and the 2D model at zero temperature ($T = 0$). In both cases, we found the coexistence region of AF order and SF.

It is then interesting to relax the above assumption of homogeneous distribution of holes and consider the

possibility of PS. With an isotropic AF coupling, it is reported[12] that the ground state of the 2D bosonic t - J model is spatially homogeneous without PS for $J/t \leq 1.5$. In this paper, we shall study the 3D bosonic t - J model at finite T in the slave-particle representation *without* the above mentioned approximation. That is, we treat the holon variables ϕ_x as genuine HCB instead of the compact Higgs field $\exp(i\varphi_x)$. We express ϕ_x as another CP^1 (pseudo) spin field $w_{x\eta}$ ($\eta = 1, 2$) via pseudo-spin $\text{SU}(2)$ operator as

$$\phi_x = w_{x2}^\dagger w_{x1}. \quad (1.3)$$

We study this double- CP^1 system of $z_{x\sigma}$ and $w_{x\eta}$ by MC simulations. We examine its phase structure, various correlation functions, and possible PS, and so on.

The present paper is organized as follows. In Sec.2, we introduce the double- CP^1 representation of the bosonic t - J model in the 3D lattice at finite T 's. We define two versions of the model, Model I directly derived from the t - J model, and Model II, a simplified version of Model I. They have different weights in spin stiffness. By comparing the results of these two models, one may obtain further understanding of the interplay of holons and spinons. In Sec.3, we exhibit the results of the numerical study and the phase diagram of the simplified mode, Model II first. We calculated the specific heat, the spin and atomic correlation functions. From these results, we conclude that there exists a coexisting phase of AF long-range order and SF in a region of low- T and intermediate hole concentrations. In Sec.4, we consider Model I and present the MC results. We compare the phase structures of the two models. We also study the PS of both models. Section 5 is devoted for conclusion. In Appendix A, we derive the expression of the HCB operator ϕ_x in terms of another CP^1 operator $w_{x\eta}$.

II. MODEL I AND MODEL II

Let us start with the bosonic Hubbard model of HCB's. Its Hamiltonian is given by

$$H_{\text{Hub}} = -t \sum_{x,\mu,\sigma} (B_{x+\mu,\sigma}^\dagger B_{x\sigma} + \text{H.c.}) + U \sum_x \hat{n}_{x1} \hat{n}_{x2},$$

$$\hat{n}_{x\sigma} \equiv B_{x\sigma}^\dagger B_{x\sigma}, \quad (2.1)$$

where $B_{x\sigma}$ is the HCB operator[13, 14] to describe the bosonic atom at the site x of the 3D cubic lattice and the spin σ [$= 1(\uparrow), 2(\downarrow)$]. $\mu(= 1, 2, 3)$ is the 3D direction index and also denotes the unit vector. $B_{x\sigma}$ satisfies the following mixed commutation relations for HCB's[15],

$$\begin{aligned} [B_{x\sigma}, B_{x\sigma'}^\dagger]_+ &= \delta_{\sigma\sigma'}, [B_{x\sigma}, B_{x\sigma'}]_+ = 0, \\ [B_{x\sigma}, B_{y\sigma'}^\dagger] &= [B_{x\sigma}, B_{y\sigma'}] = 0 \text{ for } x \neq y. \end{aligned} \quad (2.2)$$

We note that H_{Hub} has a global $\text{SU}(2)$ symmetry under

$$B_{x\sigma} \rightarrow B'_{x\sigma} = \sum_{\sigma'} g_{\sigma\sigma'} B_{x\sigma'}, \quad g \in \text{SU}(2). \quad (2.3)$$

Actually, the first term is manifestly invariant. To show that the second term is also invariant, we introduce the atomic number operator,

$$\hat{n}_x \equiv \hat{n}_{x1} + \hat{n}_{x2}, \quad (2.4)$$

which is also invariant under (2.3). Then the second term is expressed solely by this invariant quantity \hat{n}_x as

$$\begin{aligned} \hat{n}_{x1} \hat{n}_{x2} &= \frac{1}{2} (\hat{n}_{x1} + \hat{n}_{x2})^2 - \frac{1}{2} (\hat{n}_{x1}^2 + \hat{n}_{x2}^2) \\ &= \frac{1}{2} (\hat{n}_x^2 - \hat{n}_x), \end{aligned} \quad (2.5)$$

where we used the relation $\hat{n}_{x\sigma}^2 = \hat{n}_{x\sigma}$, which holds because the eigenvalue of $\hat{n}_{x\sigma}$ is 0 or 1 due to HCB.

From this Hubbard model one may derive the bosonic t - J model as its effective model for strong correlations, i.e., for large U , and small hole concentrations. The Hamiltonian H of the 3D bosonic t - J model is given by

$$\begin{aligned} H &= -t \sum_{x,\mu,\sigma} (\tilde{B}_{x+\mu,\sigma}^\dagger \tilde{B}_{x\sigma} + \text{H.c.}) \\ &\quad + J \sum_{x,\mu} \left(\vec{\tilde{S}}_{x+\mu} \cdot \vec{\tilde{S}}_x - \frac{1}{4} \hat{n}_{x+\mu} \hat{n}_x \right), \\ \tilde{B}_{x\sigma} &\equiv (1 - \hat{n}_{x\bar{\sigma}}) B_{x\sigma}, \quad (\bar{1} \equiv 2, \bar{2} \equiv 1), \\ \vec{\tilde{S}}_x &\equiv \frac{1}{2} B_x^\dagger \vec{\sigma} B_x, \quad (\vec{\sigma} : \text{Pauli matrices}). \end{aligned} \quad (2.6)$$

The derivation of (2.6) is achieved just by following the steps developed in the theory of high- T_c superconductivity to derive the fermionic t - J model from the standard Hubbard model. Actually, the second-order perturbation theory in terms of small parameter t/U produces (2.6) with the relation $J = 4t^2/U$ [16]. The role of Pauli principle for fermions is played here by the hard-core nature of bosons.

Because of the hard-core nature of $B_{x\sigma}$, $(B_{x\sigma}^\dagger)^2 = 0$, the states of double occupancy of the same-spin bosons at each site are excluded. Furthermore, as we consider the case of strong repulsion between two bosons with opposite spins at the same site, we impose another constraint that excludes from the physical space the double-occupancy state of two bosons with the opposite spins at each site. This implies the states $B_{x\uparrow}^\dagger B_{x\downarrow}^\dagger |0\rangle$ are excluded from the physical space[17]. The tilde operator $\tilde{B}_{x\sigma}$ reflects this fact. These two constraints are expressed for the normalized physical states $|\text{phys}\rangle$ as

$$\langle \text{phys} | \hat{n}_x | \text{phys} \rangle = \langle \text{phys} | \sum_{\sigma} B_{x\sigma}^\dagger B_{x\sigma} | \text{phys} \rangle \leq 1. \quad (2.7)$$

The Hamiltonian (2.6) respects $\text{SU}(2)$ symmetry (2.3). To see it, it is helpful to rewrite $\tilde{B}_{x\sigma} = (1 - \hat{n}_{x\bar{\sigma}}) B_{x\sigma} = (1 - \hat{n}_x) B_{x\sigma}$ due to $B_{x\sigma}^2 = 0$.

As mentioned, the fermionic counterpart of the present bosonic model, the (fermionic) t - J model, is a canonical model for strongly-correlated electron systems like the

high-temperature superconductors. The 2D fermionic t - J model has been studied intensively by means of various methods since the discovery of the high- T superconductors, although its phase structure etc. are still not clarified[18]. The slave-particle approach like the slave-boson or slave-fermion representations has provided us with an intuitive way of description of the t - J model in the mean field theory, in the charge-spin separated state[19], and so on. It is natural to expect that the slave-particle approach is useful also in the bosonic t - J model.

In the slave-particle representation, $B_{x\sigma}$ is expressed as

$$B_{x\sigma} = \phi_x^\dagger a_{x\sigma}. \quad (2.8)$$

ϕ_x represents the annihilation operator of the hard-core holon, and satisfies the HCB algebra of single species,

$$\begin{aligned} [\phi_x, \phi_x^\dagger]_+ &= 1, \quad [\phi_x, \phi_x]_+ = 0, \\ [\phi_x, \phi_y^\dagger] &= [\phi_x, \phi_y] = 0 \text{ for } x \neq y. \end{aligned} \quad (2.9)$$

$a_{x\sigma}$ represents annihilation operator of the bosonic spinon carrying $s = 1/2$ spin. Their commutation relations are

$$[a_{x\sigma}, a_{y\sigma'}^\dagger] = \delta_{xy}\delta_{\sigma\sigma'}, \quad [a_{x\sigma}, a_{y\sigma'}] = 0. \quad (2.10)$$

The physical-state condition (2.7) is replaced by the following equation in terms of the slave-particle operators $a_{x\sigma}$ and ϕ_x ,

$$\left(\sum_{\sigma} a_{x\sigma}^\dagger a_{x\sigma} + \phi_x^\dagger \phi_x \right) |\text{phys}\rangle = |\text{phys}\rangle. \quad (2.11)$$

Meaning of Eq.(2.11) is obvious. There are three physical states for each x ; one-holon state (holon number $\phi_x^\dagger \phi_x = 1$), corresponding to the state with no atoms, and the two one-spinon states (one with spinon number $a_{x1}^\dagger a_{x1} = 1$ and the other with $a_{x2}^\dagger a_{x2} = 1$) corresponding to the two one-atom states. The correspondence among these physical states are given as follows:

$$\begin{aligned} B_{x\sigma}|0\rangle &= 0, \\ \phi_x|\text{vac}\rangle &= a_{x\sigma}|\text{vac}\rangle = 0, \\ |0\rangle &= \phi_x^\dagger|\text{vac}\rangle, \quad \text{No - atom state} \\ B_{x\sigma}^\dagger|0\rangle &= a_{x\sigma}^\dagger|\text{vac}\rangle, \quad \text{Two one - atom states.} \end{aligned} \quad (2.12)$$

In terms of the slave-particle operators, the Hamiltonian (2.6) becomes

$$\begin{aligned} H &= -t \sum_{x, \pm\mu, \sigma} \phi_x^\dagger a_{x\pm\mu, \sigma}^\dagger a_{x\sigma} \phi_{x\pm\mu} \\ &+ \frac{J}{4} \sum_{x, \mu} [(a^\dagger \vec{\sigma} a)_{x+\mu} \cdot (a^\dagger \vec{\sigma} a)_x - (a^\dagger a)_{x+\mu} (a^\dagger a)_x], \end{aligned} \quad (2.13)$$

where we write $(a^\dagger a)_x \equiv \sum_{\sigma} a_{x\sigma}^\dagger a_{x\sigma}$, $(a^\dagger \vec{\sigma} a)_x \equiv \sum_{\sigma, \sigma'} a_{x\sigma}^\dagger \vec{\sigma}_{\sigma\sigma'} a_{x\sigma'}$.

The constraint (2.11) is solved as

$$a_{x\sigma} = (1 - \phi_x^\dagger \phi_x) z_{x\sigma}, \quad (2.14)$$

where $z_{x\sigma}$ is the CP^1 spin operator that satisfies the usual commutation relations for bosons and the following CP^1 constraint,

$$\sum_{\sigma} z_{x\sigma}^\dagger z_{x\sigma} = 1. \quad (2.15)$$

To derive Eq.(2.14) we have used the identity

$$(1 - \phi_x^\dagger \phi_x)^2 = (1 - \phi_x^\dagger \phi_x), \quad (2.16)$$

because the eigenvalues of $\phi_x^\dagger \phi_x$ are 0 and 1.

In Appendix A, we show that the HCB operator ϕ_x can be exactly expressed in terms of another CP^1 operator $w_{x\eta}$ ($\eta = 1, 2$), which satisfy the usual bosonic commutation relations and the constraint,

$$\sum_{\eta=1}^2 w_{x\eta}^\dagger w_{x\eta} = 1. \quad (2.17)$$

The expression of ϕ_x is then given by

$$\phi_x = w_{x2}^\dagger w_{x1}. \quad (2.18)$$

Then we employ the path-integral expression of the partition function

$$Z = \text{Tr} \exp(-\beta H), \quad (2.19)$$

at T with $\beta \equiv 1/(k_B T)$. For this purpose we introduce two sets of CP^1 variables, $z_{x\sigma}(\tau)$, $w_{x\eta}(\tau)$ at each site x and imaginary time $\tau \in [0, \beta \equiv (k_B T)^{-1}]$. (Hereafter we often set the Boltzmann constant k_B to unity.) They are complex numbers satisfying

$$\begin{aligned} \sum_{\sigma=1}^2 \bar{z}_{x\sigma}(\tau) z_{x\sigma}(\tau) &= 1, \\ \sum_{\eta=1}^2 \bar{w}_{x\eta}(\tau) w_{x\eta}(\tau) &= 1. \end{aligned} \quad (2.20)$$

Then the partition function is given by means of path integrals over $z_{x\sigma}(\tau)$ and $w_{x\eta}(\tau)$.

To proceed further, we make one simplification by considering finite- T region, such that the τ -dependence of the variables in the path integral can be ignored keeping only the zero modes, i.e., $z_{x\sigma}(\tau) \rightarrow z_{x\sigma}$, etc.[9]. To study the phase structure at finite T is very important because it summarizes the essential properties of the system. Besides it, finite- T phase diagram gives a very useful insight into the phase structure at $T = 0$, i.e., if some ordered states are found at finite T , we can naturally expect that they persist down to $T = 0$.

Let us present the path-integral expression Z_I of the partition function (2.19) of the 3D model at finite T 's.

$$Z_I = \int \prod_x [dz_x dw_x \prod_{\mu} dU_{x\mu}] \exp(A_I - \mu_c \sum_x \bar{\phi}_x \phi_x), \quad (2.21)$$

where the suffix I has been attached because we call this model Model I (We shall introduce Model II later). The action A_I on the 3D lattice is given by

$$\begin{aligned}
A_I &= A_s + A_h, \\
A_s &= \frac{c_1}{2} \sum_{x,\mu,\sigma} P_x P_{x+\mu} \left(\bar{z}_{x+\mu,\sigma} U_{x\mu} z_{x\sigma} + \text{c.c.} \right), \\
A_h &= \frac{c_3}{2} \left[\sum_{x,\mu,\sigma} \bar{z}_{x+\mu,\sigma} z_{x\sigma} \phi_{x+\mu} \bar{\phi}_x + \text{c.c.} \right], \\
P_x &\equiv 1 - \bar{\phi}_x \phi_x, \\
\tilde{z}_{x1} &\equiv \bar{z}_{x2}, \quad \tilde{z}_{x2} \equiv -\bar{z}_{x1} \quad (\tilde{z}_x \equiv i\sigma_2 \bar{z}_x^\dagger), \\
\phi_x &\equiv \bar{w}_{x2} w_{x1}, \quad U_{x\mu} \equiv \exp(i\theta_{x\mu}), \quad (2.22)
\end{aligned}$$

and the integration measure is

$$\begin{aligned}
\int dz_x &= \int_{-\infty}^{\infty} dz_{x1} \int_{-\infty}^{\infty} dz_{x2} \delta\left(\sum_{\sigma} \bar{z}_{x\sigma} z_{x\sigma} - 1\right) \text{ etc.}, \\
\int dU_{x\mu} &= \int_0^{2\pi} \frac{d\theta_{x\mu}}{2\pi}. \quad (2.23)
\end{aligned}$$

Here we have used the same letter ϕ_x for the complex variable and the operator in Eq.(2.9) because no confusions arise. According to Ref.[9], we have introduced the U(1) gauge field $U_{x\mu} \equiv \exp(i\theta_{x\mu})$ on the link $(x, x + \mu)$ as an auxiliary field to make the action in a simpler form and the U(1) gauge invariance manifest.

The term $-\mu_c \sum_x \bar{\phi}_x \phi_x$ with the (minus of) chemical potential μ_c has been introduced to control the hole density ρ ,

$$\rho(c_1, c_3, \mu_c) \equiv \frac{1}{N} \sum_x \langle \bar{\phi}_x \phi_x \rangle, \quad (2.24)$$

where $N = \sum_x 1$ is the total number of the sites. As indicated, $\rho(c_1, c_3, \mu_c)$ is a function of c_1, c_3 and μ_c . We are interested in the case that the hole density ρ takes a constant value δ as c_1, c_3, μ_c are varied, because each material has a constant hole density, δ . Then, to obtain a physical quantity for given c_1, c_3 and δ , we determine μ_c so that the relation

$$\rho(c_1, c_3, \mu_c) = \delta, \quad (2.25)$$

holds. It implies to determine $\mu_c(c_1, c_3, \delta)$ as a function of c_1, c_3, δ .

Because the equation

$$\hat{n}_x = 1 - \phi_x^\dagger \phi_x, \quad (2.26)$$

holds for the physical states, there is a relation among the atomic density n and the hole density ρ as

$$n \equiv \frac{1}{N} \langle \sum_x \hat{n}_x \rangle = 1 - \rho, \quad (2.27)$$

as expected.

The action A_I of (2.22) has the global SU(2) spin symmetry of (2.3),

$$\begin{aligned}
z_x &\rightarrow g z_x, \quad g \in \text{SU}(2) \\
\bar{z}_{x+\mu} z_x &\rightarrow \bar{z}_{x+\mu} \bar{g} g z_x = \bar{z}_{x+\mu} z_x, \\
\bar{z}_{x+\mu} z_x &\rightarrow \det g \cdot \bar{z}_{x+\mu} z_x = \bar{z}_{x+\mu} z_x. \quad (2.28)
\end{aligned}$$

We note that the present model may describe not only $s = 1/2$ case but also the case with an *arbitrary* s . In this case, Eq.(2.20) becomes as[20]

$$\sum_{\sigma=1}^2 \bar{z}_{x\sigma} z_{x\sigma} = 2s, \quad (2.29)$$

but the above normalization factor $2s$ can be easily absorbed into the parameters c_1 and c_3 in the action.

The action A_I is also invariant under a local (x -dependent) U(1) gauge transformation,

$$\begin{aligned}
z_{x\sigma} &\rightarrow e^{i\lambda_x} z_{x\sigma}, \quad \phi_x \rightarrow e^{i\lambda_x} \phi_x, \\
U_{x\mu} &\rightarrow e^{-i\lambda_{x+\mu}} U_{x\mu} e^{-i\lambda_x}, \\
w_{x1} &\rightarrow e^{i\frac{\lambda_x}{2}} w_{x1}, \quad w_{x2} \rightarrow e^{-i\frac{\lambda_x}{2}} w_{x2}, \quad (2.30)
\end{aligned}$$

where λ_x is an arbitrary function. The complex variable $B_{x\sigma}$ [21] for the gauge-invariant *bosonic* atoms is expressed in terms of z_σ and w_η as

$$B_{x\sigma} = \bar{\phi}_x z_{x\sigma} = \bar{w}_{x1} w_{x2} z_{x\sigma}. \quad (2.31)$$

The parameters c_1 and c_3 are related with those in the original t - J model as[9]

$$\begin{aligned}
c_1 &\sim \begin{cases} J\beta & \text{for } c_1 \gg 1, \\ (2J\beta)^{1/2} & \text{for } c_1 \ll 1, \end{cases} \\
c_3 &\sim t\beta. \quad (2.32)
\end{aligned}$$

Note that c_3 here has no extra factor δ compared with c_3 defined in Ref.[9].

This model (2.22), which we call Model I, is examined in Sect.4 as announced. Before that, we study a simplified model, Model II, which is defined by setting $P_x = 1$ in (2.22). The partition function Z_{II} of Model II is then given by

$$\begin{aligned}
Z_{II} &= \int \prod_x [dz_x dw_x \prod_{\mu} dU_{x\mu}] \exp(A_{II} - \mu_c \sum_x \bar{\phi}_x \phi_x), \\
A_{II} &= A'_s + A_h, \\
A'_s &= \frac{c_1}{2} \sum_{x,\mu,\sigma} \left(\bar{z}_{x+\mu,\sigma} U_{x\mu} z_{x\sigma} + \text{c.c.} \right). \quad (2.33)
\end{aligned}$$

The main reason to study Model II is to clarify the effect of the projection operator to the hole-free states, P_x , by comparing the results of the two models. We expect that the AF ordered state appears with stronger signals in Model II than in Model I because the assignment $P_x = 1$ in Model II lets the AF coupling between the nearest-neighbor (NN) spin pairs at $(x, x + \mu)$ survive even if a hole occupies the sites x and/or $x + \mu$. Here we note that, in the path-integral formulation, the variable $z_x(\tau)$

is defined for all (x, τ) even if the site x is totally occupied by a hole[22]. Due to the short-range AF configuration, such z_x reflects a nearby spin orientation. In other words, Model II effectively describes a doped AF Heisenberg model with, e.g., next-NN exchange couplings that enhance AF long-range order.

III. RESULTS OF MC SIMULATIONS OF MODEL II

In this section, we present the results of MC simulations for Model II of (2.33). For MC simulations, we consider a 3D cubic lattice of the size $N \equiv L^3$ (L up to 36) and imposed the periodic boundary condition. We used the standard Metropolis algorithm with local updates. Average number of sweeps was 12×10^4 , and average acceptance ratio was about 40%~70%.

A. Phase structure

Let us first discuss the phase structure. To this end, we measured the internal energy U , the specific heat C and the hole density ρ defined as

$$\begin{aligned} U &= -\frac{1}{N} \langle A \rangle, \\ C &= \frac{1}{N} (\langle A^2 \rangle - \langle A \rangle^2), \\ \rho &= \frac{1}{N} \langle \sum_x \bar{\phi}_x \phi_x \rangle. \end{aligned} \quad (3.1)$$

In Fig.1 we show the obtained phase diagram in the c_3 - c_1 plane for various values of $\rho = \delta$. The phase transition lines in Fig.1 were determined by the measurement of U and C in (3.1). We found that there are four phases listed in Table 1. The nature of each phase was confirmed by measuring various correlation functions, which we shall discuss in the following subsection in detail.

Let us present a qualitative understanding of the phase diagram Fig.1. For this purpose, it is convenient to introduce an O(3) spin vector $\vec{\ell}_x$ made of spinon z_x ,

$$\vec{\ell}_x \equiv \bar{z}_x \vec{\sigma} z_x, \quad \vec{\ell}_x \cdot \vec{\ell}_x = 1, \quad (3.2)$$

where summations over spin indices are understood. The short-range (SR) spin correlation $\vec{\ell}_{x+\mu} \cdot \vec{\ell}_x$ is expressed by the SR CP¹ amplitude (such as $\bar{z}_{x+\mu} z_x$) as

$$\vec{\ell}_{x+\mu} \cdot \vec{\ell}_x = 2|\bar{z}_{x+\mu} z_x|^2 - 1 = -2|\bar{z}_{x+\mu} z_x|^2 + 1, \quad (3.3)$$

AF:	Antiferromagnetic phase
PM:	Paramagnetic phase
AF+SF:	Phase of antiferromagnetism and SF
FM+SF:	Phase of ferromagnetism and SF

Table 1. Various phases in Fig.1

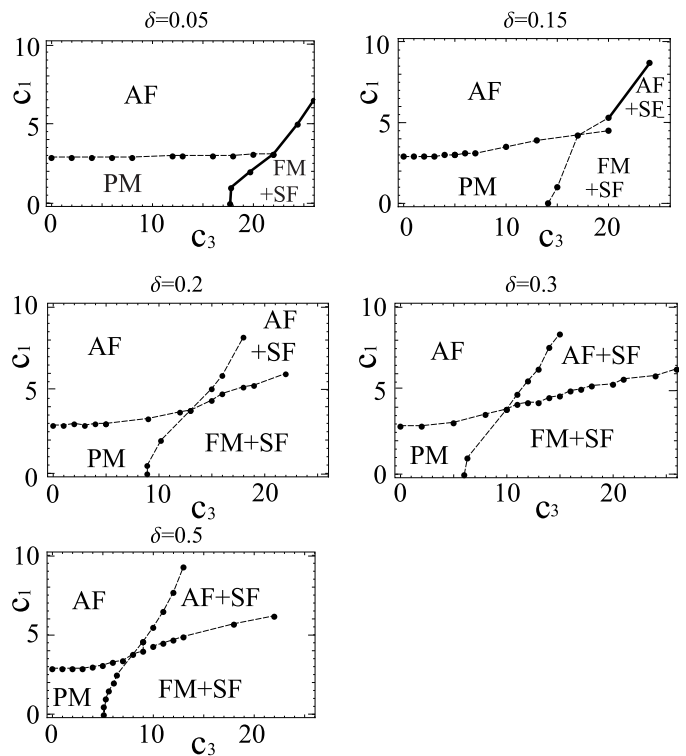


FIG. 1. Phase structure of Model II in the c_3 - c_1 plane for various δ . The meaning of abbreviations for each phase is listed in Table 1. The phase transition into the FM+SF phase for $\delta = 0.05$ and the phase transition between the AF and AF+SF phases for $\delta = 0.15$ (solid curves) are of first order. All the other transitions (dashed curves) are of second order.

where z_x satisfies

$$|\bar{z}_{x+\mu} z_x|^2 + |\bar{z}_{x+\mu} z_x|^2 = 1. \quad (3.4)$$

So the SRAF configuration $\vec{\ell}_{x+\mu} \cdot \vec{\ell}_x \simeq -1$ corresponds to $|\bar{z}_{x+\mu} z_x| \simeq 1$, and the SRFM configuration $\vec{\ell}_{x+\mu} \cdot \vec{\ell}_x \simeq 1$ corresponds to $|\bar{z}_{x+\mu} z_x| \simeq 1$. The c_1 term A'_s of (2.33) controls the spin fluctuations and the AF order ($|\bar{z}_{x+\mu} z_x| \simeq 1$) is generated for sufficiently large values of c_1 . The c_3 term A_h of (2.22), (2.33) controls the rate of hopping of holons, $\phi_{x+\mu}^\dagger \phi_x$, accompanied with a SRFM spinon amplitude $z_{x+\mu} \bar{z}_x$. The SF of holons is generated for sufficiently large values of c_3 if there exists a sufficient amount of FM spin amplitude $\langle z_{x+\mu} \bar{z}_x \rangle$. Therefore, for sufficiently large values of c_3 , we expect a coherent SF of holons accompanied with a (SR) FM order. As the results in Fig.1 show, there exists the coexisting phase of AF and SF for intermediate and large hole density. More details of the spin configuration in this phase will be given in the following sections.

In Fig.2 we show the phase diagram drawn in the $\delta - 1/c_1$ plane for several values of c_3/c_1 . The value for vertical axis, $1/c_1$, and the ratio c_3/c_1 are expressed

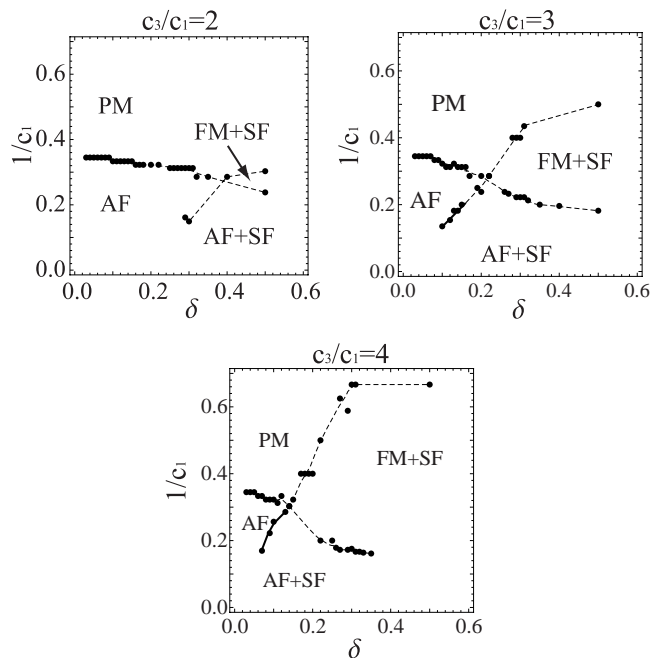


FIG. 2. Phase structure of Model II in the δ - $1/c_1$ plane ($1/c_1 \sim k_B T/J$) for $c_3/c_1 (\sim t/J) = 2.0, 3.0, 4.0$. The abbreviations for each phase are listed in Table 1. The phase transition between the AF and AF+SF phases for $c_3/c_1 = 3.0, 4.0$ drawn in solid curves are of first order. All the other transitions drawn in dashed curves are of second order.

for $c_1 \gg 1$ from (2.32) as

$$\frac{1}{c_1} \sim \frac{1}{J\beta} \sim \frac{k_B T}{J}, \quad \frac{c_3}{c_1} \sim \frac{t}{J}. \quad (3.5)$$

So Fig.2 may be interpreted as the phase diagram in the $\delta - T$ plane[23]. The Néel temperature $T_N(\delta)$ (the critical temperature of the AF transition) decreases as holons are doped (as δ increases). The rate of reduction $-dT_N(\delta)/d\delta$ increases as t/J increases because the movement of holons becomes significant to destroy AF order. The critical temperature $T_{SF}(\delta)$ for SF of holons increases as δ increases as expected. The rate of increase $dT_{SF}(\delta)/d\delta$ also rises as t/J increases, because the movement of holons favors their homogeneous distribution and so their SF.

Let us examine some details of the phase transitions in Fig.1. First, we focus on the transition from the PM phase to the AF phase that takes place as the value of c_1 is increased. In Fig.3 we present U , C and ρ along $c_3 = 4.0$, $\delta \simeq 0.10$ to locate the transition point between the PM and AF phases. It seems that the phase transition is of second order because there are no hysteresis in U and the peak of C develops systematically as L increases. We obtained similar behavior of U and C in the PM-AF phase transition for cases of other values of δ shown in Fig.1.

Secondly, we examine the transition between the PM phase and the FM+SF phase. In Fig.4 we present U , C along $c_1 = 1.5$ and $\mu_c = 10.0$, which indicate a second-

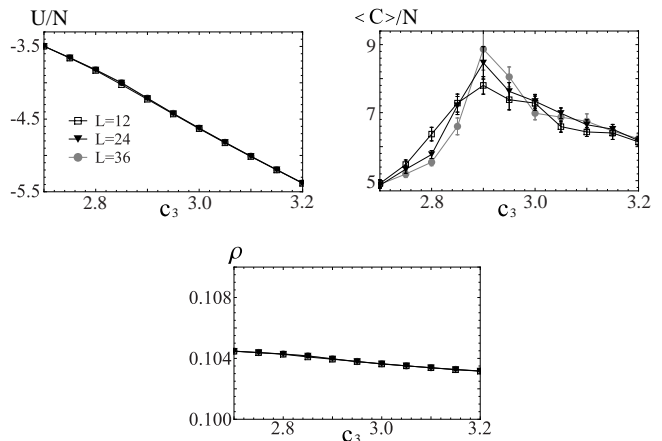


FIG. 3. E , C and ρ along $c_3 = 4.0$ and $\delta \simeq 0.10$. A transition between the PM and AF phases exists at $c_1 \simeq 2.9$. Corresponding value of chemical potential $\mu_c = 10$.

order transition at $c_3 \simeq 9.0$ between the PM and FM+SF phases. ρ increases as c_3 increases crossing the transition point.

Thirdly, we examine the transition between the AF and AF+SF phases at $\delta \simeq 0.15$. In Fig.5 we show U , C , ρ for $c_3 = 24.0$ and $\mu_c = 16.0$. There are hysteresis curves in these quantities, which indicate a first-order phase transition. Similar first-order transitions are found also for $\delta = 0.05$ and $\delta = 0.15$ as indicated by solid curves in Fig.1. We determined the transition point from the hysteresis data by averaging the two values of ρ for fixed μ_c, c_1, c_3, ρ_1 on the upper hysteresis curve and ρ_2 on the lower hysteresis curve, so that

$$a_1 \rho_1 + a_2 \rho_2 = \delta, \quad a_1 + a_2 = 1, \quad (3.6)$$

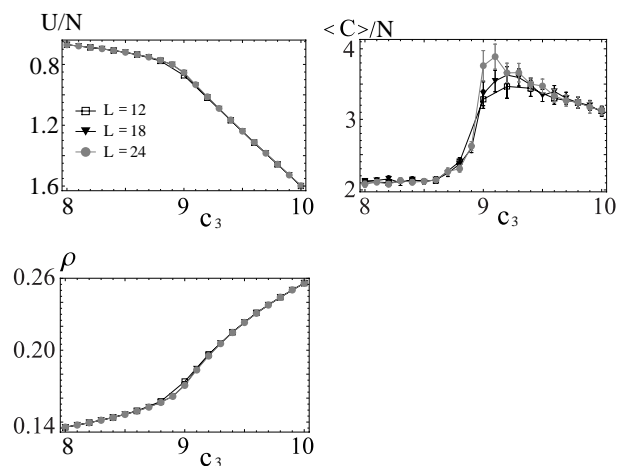


FIG. 4. U , C along $c_1 = 1.5$ and $\mu_c = 10.0$. A second-order transition between the PM and FM+SF phases exists at $c_3 \simeq 9.0$.

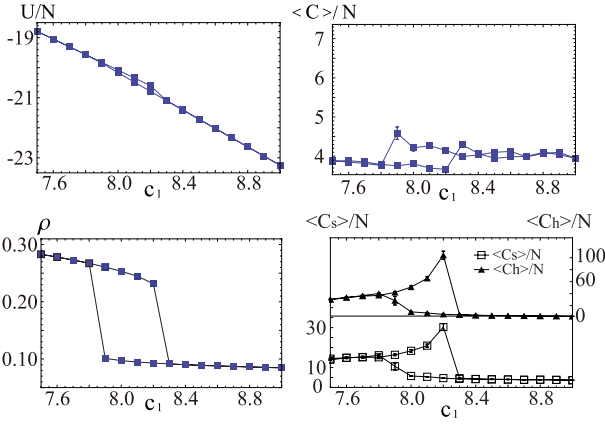


FIG. 5. U , C , ρ vs c_1 for $c_3 = 24.0$ and $\mu_c = 16.0$ ($L = 12$). A first-order transition between the AF and AF+SF phases exists at $c_1 \simeq 8.2$.

to obtain the given value of δ . U and C are averaged with these weights a_1, a_2 .

Finally, we examine the successive transitions from the FM+SF phase to the AF+SF phase and then to the AF phase. In Fig.6 we present U, C along $c_3 = 16.0$ and $\mu_c = 10.0$. We see that there is only one peak in C at $c_1 \simeq 5.0$ that corresponds to the transition between the FM+SF phase and the AF+SF phase, the peak for the transition from the AF+SF phase to the AF phase being missing. (For identification of these phases, see later discussion.) However the hole density ρ changes its behavior at $c_1 \simeq 5.9$, while C exhibits only very small anomalous behavior (dip) at that point.

To clarify the possible transition at $c_1 \simeq 5.9$, we measured the “separate specific heats” for the A'_s term and

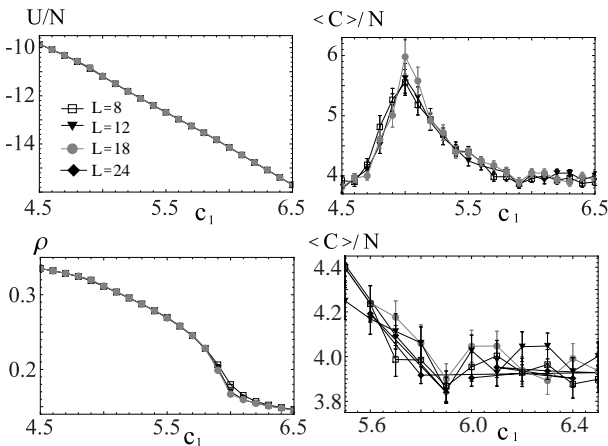


FIG. 6. U , C , ρ along $c_3 = 16.0$ and $\mu_c = 10.0$. A second-order transition between the FM+SF and AF+SF phases exists at $c_1 \simeq 5.0$. There is a dip in C at $c_1 \simeq 5.9$, which suggests another transition (See Fig.7 and the text).

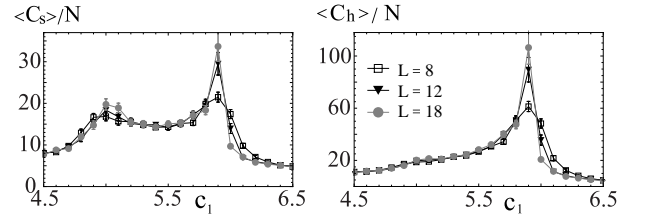


FIG. 7. The specific heat for each term, C_s , C_h along $c_3 = 16.0$ and $\mu_c = 10.0$. They exhibit the corresponding peaks (or cusp) for the transition between the FM+SF and AF+SF phases and the transition between the AF+SF and AF phases.

the A_h term separately. They are defined as

$$C_s = \frac{1}{N} (\langle A_s^2 \rangle - \langle A_s \rangle^2),$$

$$C_h = \frac{1}{N} (\langle A_h^2 \rangle - \langle A_h \rangle^2). \quad (3.7)$$

In Fig.7 we present C_s and C_h separately. Both C_h and C_s exhibit a very sharp peak at $c_1 \simeq 5.9$. This kind of “cancellation” of specific heats of each term in the total specific heat C has been observed sometimes. This stems from the fact that $\langle A'_s \rangle$ is an increasing function of c_1 whereas $\langle A_h \rangle$ is a decreasing function of c_1 . At $c_1 \simeq 5.9$, cancellation between these two terms occurs and $\langle A_{II} \rangle$ becomes a smooth function of c_3 . The study of correlation function in the next subsection shows a possible phase transition between AF+SF and AF phases at $c_1 \simeq 5.9$.

B. Correlation functions

In the previous subsection, we showed the phase diagrams for various hole density. In order to understand physical properties of each phase, let us study some correlation functions. Because the spin operator \vec{S}_x of atom is given by Eq.(2.6) as

$$\vec{S}_x = \frac{1}{2} B_x^\dagger \vec{\sigma} B_x = \frac{1}{2} (1 - \phi_x^\dagger \phi_x) z_x^\dagger \vec{\sigma} z_x, \quad (3.8)$$

we define the corresponding normalized classical atomic spin vector,

$$\vec{\ell}_x \equiv (1 - \bar{\phi}_x \phi_x) \vec{\ell}_x, \quad (3.9)$$

using the pure O(3) spin vector $\vec{\ell}_x = \bar{z}_x \vec{\sigma} z_x$ of Eq.(3.2). We also introduce the atomic density n_x corresponding to Eq.(2.26),

$$n_x \equiv 1 - \bar{\phi}_x \phi_x. \quad (3.10)$$

Then we measure the following correlation functions,

$$\begin{aligned}
G_\ell(r) &= \frac{1}{3N} \sum_{x,\mu} \langle \vec{\ell}_{x+r\mu} \cdot \vec{\ell}_x \rangle, \\
G_B(r) &= \frac{1}{6N(1-\delta)} \sum_{x,\mu,\sigma} \langle \vec{B}_{x+r\mu,\sigma} B_{x\sigma} \rangle, \\
G_n(r) &= \frac{1}{3N(1-\delta)^2} \sum_{x,\mu} \langle n_{x+r\mu} n_x \rangle, \\
G_S(r) &= \frac{1}{3N(1-\delta)^2} \sum_{x,\mu} \langle \vec{S}_{x+r\mu} \cdot \vec{S}_x \rangle. \quad (3.11)
\end{aligned}$$

From above, they are the spin correlation of spinons, atomic correlation, density correlation, and the spin correlation of atoms, respectively. Their prefactors are chosen so that $G(r)$ is normalized as $G(0) = 1$.

In Table 2, each phase is characterized by the (non)vanishing off-diagonal long-range orders (LRO) $G(\infty)$ and/or staggered magnetizations $\tilde{G}(\infty)$,

$$\begin{aligned}
G(\infty) &\equiv \lim_{r \rightarrow \infty} G(r), \\
\tilde{G}(\infty) &\equiv \lim_{r \rightarrow \infty} (-)^r G(r), \quad (3.12)
\end{aligned}$$

measured by these correlation functions.

To show these correlation functions, we select a typical point in the c_3 - c_1 plane for each phase as in Table 3. In Fig.8 we present the four correlation functions of (3.11) at the four selected points in Table 3 for three typical values of $\delta = 0.15, 0.20$ and 0.30 . From this result, we identified each phase as in Fig.1. In the FM+SF phase and the AF+SF phase, the region $0.08 \lesssim \delta \lesssim 0.2$ requires a difficult fine tuning of μ_c . So, to obtain the correlation data for $\delta = 0.15$ in these two phases, we used the superposition (3.6) by using the data for $\delta \simeq 0.08$ and $\delta \simeq 0.2$.

The results in Fig.8 shows that the spin correlation $G_\ell(r)$ and the atomic-spin correlation $G_S(r)$ exhibit similar behavior in all phases. They have staggered magne-

	$G_{\ell,S}(\infty)$	$G_B(\infty)$	$G_n(\infty)$
PM	= 0	= 0	$\neq 0$
FM+SF	$\neq 0$	$\neq 0$	$\neq 0$
AF	SM	= 0	$\neq 0$
AF+SF	SM	$\neq 0$	$\neq 0$

Table 2. (Non)Existence of LRO in each phase. ‘‘SM’’ implies a nonvanishing staggered magnetization, $\tilde{G}(\infty)$.

phase	c_3	c_1
PM	4.0	2.0
FM+SF	24.0	2.0
AF	4.0	8.0
AF+SF	24.0	8.0

Table 3. Data points of correlation functions for each phase in the c_3 - c_1 plane.

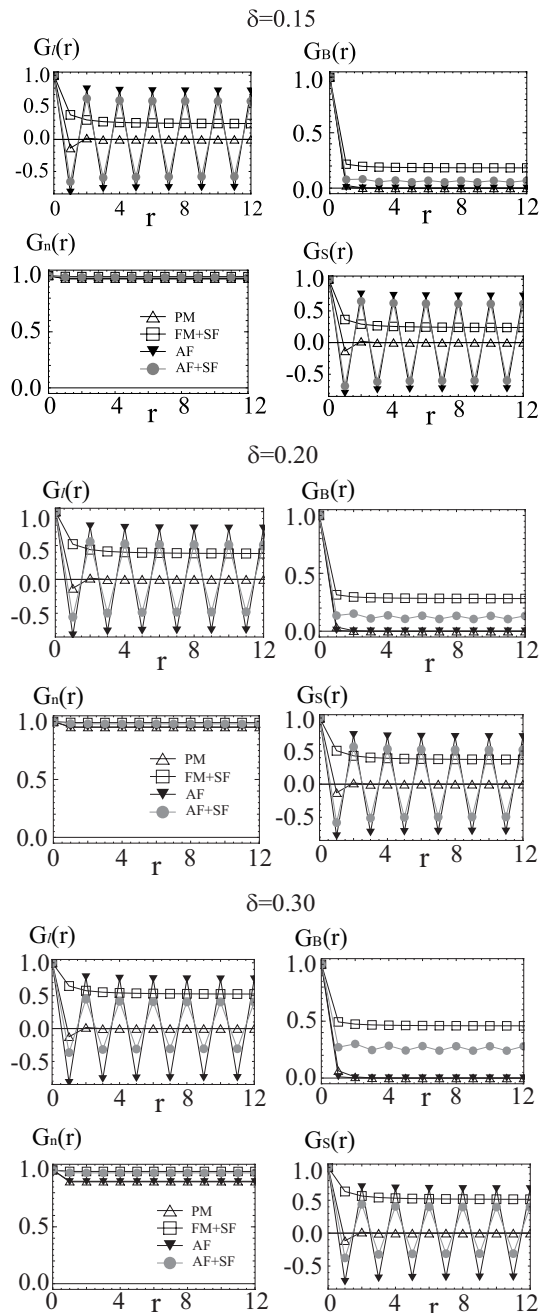


FIG. 8. Four correlation functions (3.11) at the four selected points in Table 3 for $\delta = 0.15, 0.20$ and 0.30 . They are used to identify the phases of Fig.1 according to Table 2.

tizations in the AF and AF+SF phases. The atomic correlation $G_B(r)$ has nonvanishing LRO in the FM+SF and AF+SF phases, which indicates the SF of atoms. In particular, in the AF+SF phase, $G_B(r)$ of even-even (odd-odd) sites is slightly different from that of even-odd sites, reflecting the AF nature. The atomic density correlation $G_n(r)$ shows smooth and homogeneous distribution of atoms and holes at all the examined cases of c_1, c_3, δ , indicating nonexistence of the PS phenomenon

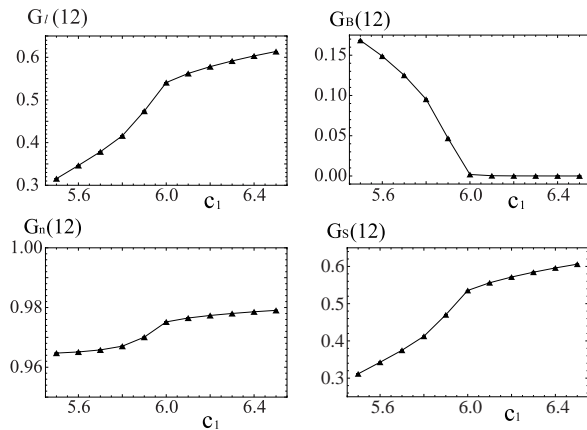


FIG. 9. Four correlation functions (3.11) at the long distance limit $G(L/2)$ vs c_1 for $c_3 = 16.0$ and $\mu_c = 10.0$. These values correspond to Figs.6,7. $G_B(L/2)$ shows a behavior of a second-order phase transition at $c_1 \simeq 5.9 \sim 6.0$.

in the present model. This point will be discussed rather in detail in the following section.

To study the possible phase transition between AF+SF and AF phases, we measured the correlation functions across the relevant region of c_1 . In Fig.9 we plot their values at long-distance limit, $G(L/2)$ for $c_3 = 16.0$ and $\mu_c = 10.0$. Because $G_B(L/2)$ decreases continuously as c_1 increases and vanishes at $c_1 \simeq 5.9 \sim 6.0$, we judge that there is a second-order phase transition from the AF+SF phase to the AF phase. Other three values $G(L/2)$ remain finite as expected from Table 2. Similarly, Fig.10 shows $G(L/2)$ for $c_3 = 16.0$ and $\mu_c = 16.0$. Again $G_B(L/2)$ decreases and vanishes but discontinuously with hysteresis. This supports our phase diagram, Fig.1, with the first-order AF+SF \leftrightarrow AF transition at $c_1 \simeq 8.2$.

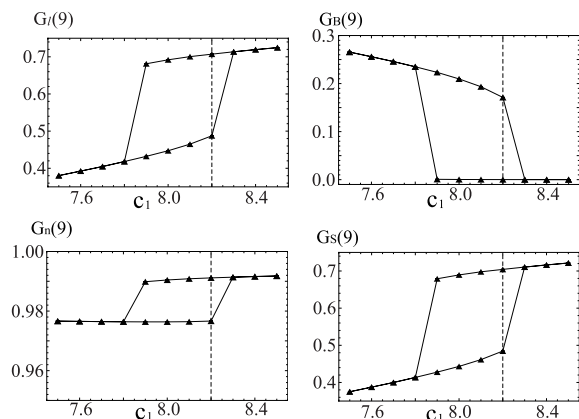


FIG. 10. Four correlation functions (3.11) at the long distance limit $G(L/2)$ vs c_1 for $c_3 = 24.0$ and $\mu_c = 16.0$. These values correspond to Fig.5. $G_B(L/2)$ shows a behavior of a first-order phase transition at $c_1 \simeq 8.2$ (dashed line), which is determined from the specific heat of Fig.5 using (3.6).

IV. RESULTS OF MC SIMULATIONS OF MODEL I

In this section, we shall study Model I of (2.22). Physical meaning of the prefactor $P_x = 1 - \bar{\phi}_x \phi_x$ in A_s of (2.22) is obvious, i.e., if the site x is occupied by a holon, the AF coupling on the link $(x, x \pm \mu)$ is suppressed. This bond-breaking effect of holons in the AF background generates an effective attractive force favoring holon pairs sitting at NN sites. Actually, a NN holon pair breaks eleven AF bonds while two holons separated by more than NN sites break twelve AF bonds [24]. This effective force can be an origin of the superconducting NN holon-pair condensation[10] and/or of a PS of holon-rich regions and holon-free (holon-poor) regions. In this section, we shall study how the phase diagram is influenced by this AF bond-breaking effect by holons, in particular, if there appears a phase-separated state.

A. Phase structure

As for Model II, we studied Model I by means of the MC simulations. In Figs.11, we show the obtained phase diagram in the $c_3 - c_1$ plane for fixed values of μ_c . There

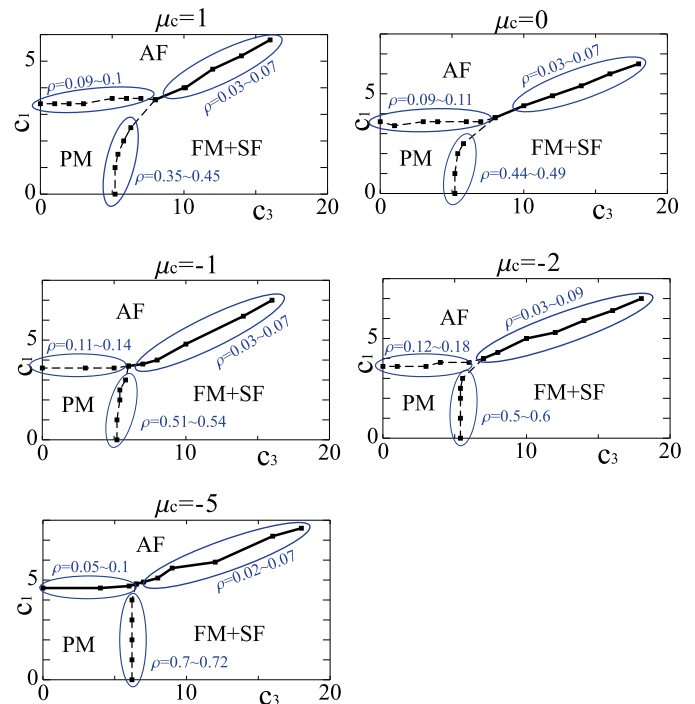


FIG. 11. Phase diagram of Model I in the $c_3 - c_1$ plane for fixed values of the chemical potential, $\mu_c = +1.0, 0.0, -1.0, -2.0, -5.0$. Hole density ρ is also shown for corresponding regions. The solid curves show first-order transitions and the dashed curves show second-order transitions. The AF+SF phase is missing.

exist the AF, PM and FM+SF phases as in Model II with low-hole doping. In the phase diagram, we also indicate the hole density δ . We found that hole density in the AF phase is rather small compared with Model II. This is due to the factor P_x in the c_1 -term of (2.22). As explained in the beginning of this section, a hole sitting on the site x makes $P_x = 0$ and suppresses the AF couplings around x . So hole doping costs larger energy in Model I than in Model II. In other words, as the hole density is increased, the AF state becomes more unstable because the AF couplings are weakened by the prefactor $P_{x+\mu}P_x$. By the numerical studies of Model I, we have concluded that the coexisting phase AF+SF of AF order and SF does not exist in Model I.

Order of each phase transition is indicated in Fig.11. In particular, the transition between the AF and FM+SF is of first order. This result is physically expected as these two phases have different LRO's in contrast. We also found that the spin correlation G_ℓ , atomic correlation G_B , etc. exhibit a similar behavior to those in Model II.

B. Phase separation and hole distribution

The PS is a phenomenon of inhomogeneous distribution of holes in which the lattice is separated into hole-rich regions and spin-rich (hole-free) regions. To study the possibility of PS, we introduced the following two quantities,

$$\begin{aligned}\Delta &= \frac{1}{N\rho^2} \sum_x \langle (\bar{\phi}_x \phi_x - \rho)^2 \rangle, \\ \Delta_c &= \frac{1}{3N\rho^2} \sum_{x,\mu} \langle (\bar{\phi}_{x+\mu} \phi_{x+\mu} - \rho)(\bar{\phi}_x \phi_x - \rho) \rangle \\ &= \frac{1}{3N\rho^2} \sum_{x,\mu} \langle \bar{\phi}_{x+\mu} \phi_{x+\mu} \bar{\phi}_x \phi_x - \rho^2 \rangle.\end{aligned}\quad (4.1)$$

The quantity Δ measures the fluctuation of hole density $\bar{\phi}_x \phi_x$ around its average ρ . As explained in (2.12), a physical state at a specific site x is a superposition of the one-holon state $|0\rangle$ ($B_{x\sigma}|0\rangle = 0$) and the no-holon states $B_{x\sigma}^\dagger|0\rangle$. When the system is with homogeneous distribution of holes like the holon-condensed state, $\bar{\phi}_x \phi_x - \rho \sim 0$ and $\Delta \sim 0$. On the other hand, when the system enters into an inhomogeneous hole-localized state, $\bar{\phi}_x \phi_x - \rho \sim -\rho$ for hole-free sites and $\bar{\phi}_x \phi_x - \rho \sim 1 - \rho$ for sites occupied by holes, and Δ develops from zero.

Similarly, Δ_c measures correlation of fluctuations of hole densities at the NN sites. When the deviation of hole densities from their average, $\bar{\phi}_x \phi_x - \rho$, at NN sites have similar values (same signs), Δ_c develops a value of $O(1)$. A hole-rich region contributes amount of $\sim (1 - \rho)^2$ to Δ_c and a hole-free region contributes $\sim \rho^2$. If $\bar{\phi}_x \phi_x$ takes finite but random values site by site, $\Delta_c \sim 0$ although $\Delta \sim O(1)$. In the phase-separated state, both Δ and Δ_c should take values of $O(1)$.

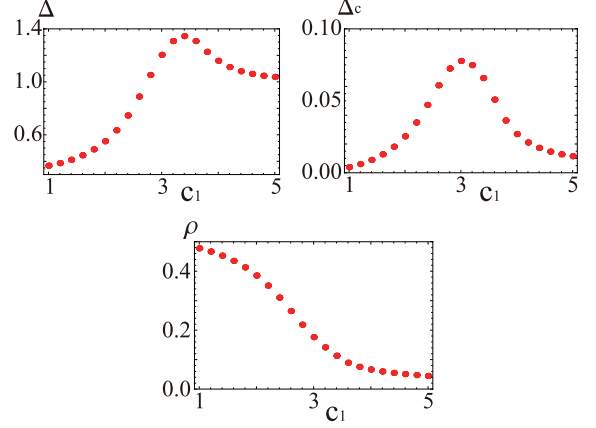


FIG. 12. Δ and Δ_c of (4.1) in Model I for $c_3 = 1.0$ and $\mu_c = 0.0$ vs c_1 . They have peaks around the phase transition point between the PM and AF phases, $c_1 \simeq 3.6$.

In Fig.12, we first show Δ , Δ_c and ρ of Model I vs c_1 for $c_3 = 1.0$ and $\mu_c = 0.0$. A phase transition from the PM to AF phases takes place at $c_1 \simeq 3.6$. Both Δ and Δ_c exhibit peaks around the transition point, though the magnitude of Δ_c itself is very small for all c_1 's. This behavior around the transition point can be understood as a result of formation of AF domains of finite sizes in the PM phase on approaching to the AF phase boundary. In the AF phase, Δ has a fairly large value, which indicates that localization of holes takes place there. However, the small Δ_c means that the PS does not take place in both AF and PM phases. ρ decreases rapidly in the AF region because holes break the AF bonds around them as explained before, costing higher energy in the AF phase than in the PM phase.

The above results should be compared with results in Model II. See Fig.13 for Model II with $c_3 = 5.0$, $\mu_c = 10.0$, in which the PM \leftrightarrow AF transition takes place and

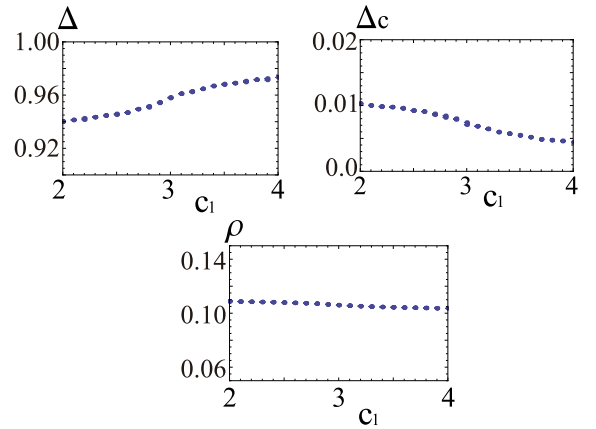


FIG. 13. Δ and Δ_c in Model II for $c_3 = 5.0$, $\mu_c = 10.0$ vs c_1 . The transition between the PM and AF phases takes place at $c_1 \simeq 2.9$.

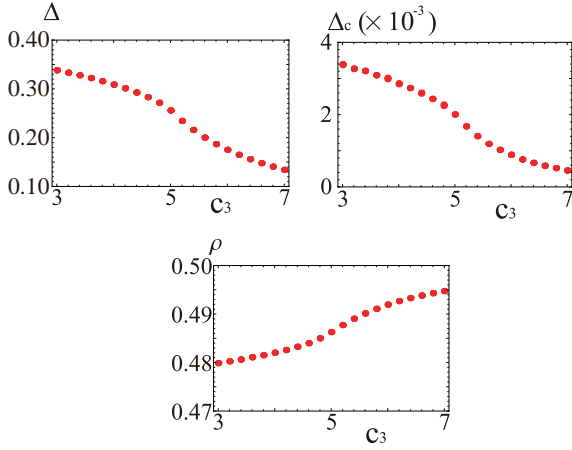


FIG. 14. Δ and Δ_c in Model I vs c_3 for $c_1 = 1.0$, $\mu_c = 0.0$. The PM \leftrightarrow FM+SF phase transition takes place at $c_3 \simeq 5.5$.

the hole density ρ takes almost the same value with that in the AF phase of Model I. However, Δ and Δ_c are almost constant while c_1 is varied across the phase transition from the PM to AF phases. In Model II, the spin dynamics does not influence the hole dynamics for sufficiently small δ . Obviously, the PS does not take place in Model II as in Model I.

Let us next see the results around the phase transition from the PM to FM+SF phases. In Fig.14, we show the results of Model I for $c_1 = 1.0$, $\mu_c = 0.0$. The hole density δ is fairly large, and both Δ and Δ_c are decreasing functions of c_3 . This result is expected, as holes in the SF phase are distributed homogeneously through the whole system. The corresponding results in the Model II for $c_1 = 1.0$ and $\mu_c = 10.0$ are given in Fig.15. Though the above parameters have different values from those in Fig.14, the same PM \leftrightarrow FM+SF phase transition takes place at $c_3 \simeq 8.5$. Δ exhibits similar behavior to that of the Model I, whereas Δ_c has a small peak at the phase

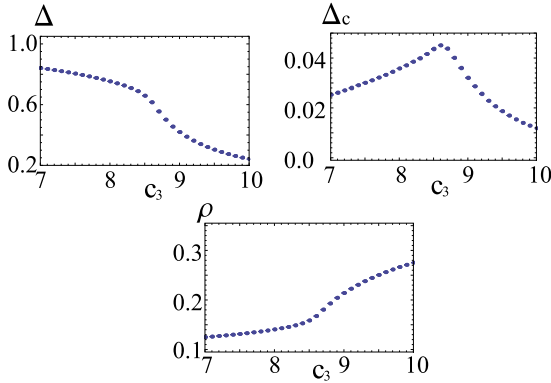


FIG. 15. Δ and Δ_c in Model II vs c_3 for $c_1 = 1.0$, $\mu_c = 10.0$. The PM \leftrightarrow FM+SF phase transition takes place at $c_3 \simeq 8.5$.

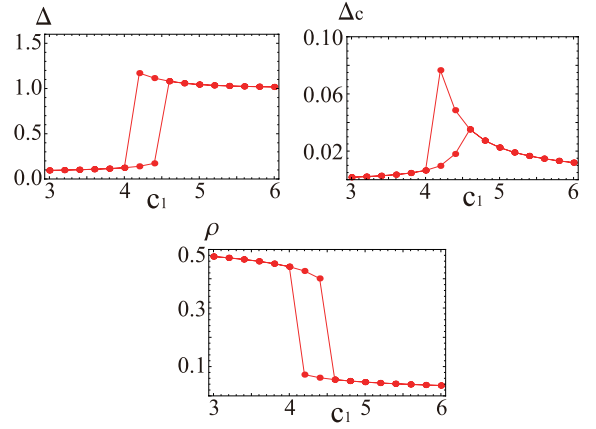


FIG. 16. Δ and Δ_c in Model I vs c_1 for $c_3 = 10.0$, $\mu_c = 0.0$. The FM+SF \leftrightarrow AF phase transition take a place at $c_1 \simeq 4.2$.

transition point.

Finally, we show Δ and Δ_c around the FM+SF \leftrightarrow AF phase transition. See Fig.16 for Model I with $c_3 = 10.0$, $\mu_c = 0.0$. Both quantities exhibit hysteresis loops around the transition point $c_1 \simeq 4.2$, because the phase transition is of first order. In the AF phase, holes are strongly localized, whereas they have a homogeneous distribution in the FM+SF phase. Corresponding numerical results for the Model II with $c_3 = 16.0$, $\mu_c = 10.0$ are given in Fig.17. There exist no anomalous behavior at the transition FM+SF \leftrightarrow AF+SF at $c_1 \simeq 5.0$, because the SF takes place in both phases. On the other hand, Δ develops in the AF phase as the SF disappears there.

To close this section, we compare our results with other works. Our conclusion that there are no PS states is compatible with the results of Ref.[6] for the isotropic 2D model at low T 's, although our system is 3D at finite

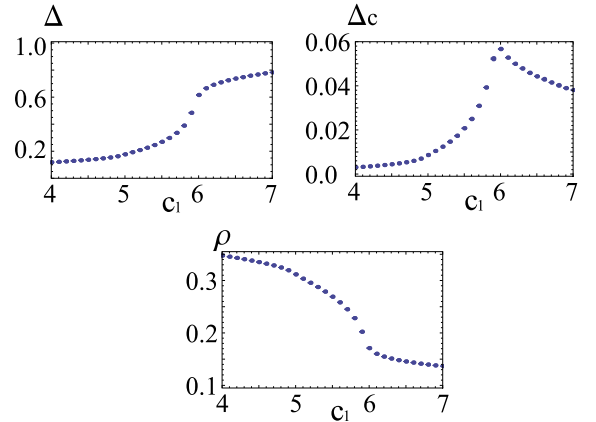


FIG. 17. Δ and Δ_c in Model II vs c_1 for $c_3 = 16.0$, $\mu_c = 10.0$. The FM+SF \leftrightarrow AF+SF and AF+SF \leftrightarrow AF phase transitions take place at $c_1 \simeq 5.0$ and $c_1 \simeq 5.9$, respectively. See Fig.7.

T 's. As mentioned in Sect.1, Boninsegni and Prokof'ev[8] studied the 2D bosonic $t-J$ model with anisotropic spin coupling ($J_{x,y} = \alpha J_z, \alpha < 1$) with $0 < J/t < 1$ at low T 's, and found PS for low hole concentrations, $\delta < \delta_c(\alpha)$, where $\delta_c(\alpha)$ is the critical density of holes and $\delta_c(\alpha) \rightarrow 0$ as $\alpha \rightarrow 1$. This implies that anisotropy is essential for PS; the stability of spins in z -direction via the NN spin coupling favors to form spin-rich regions.

V. CONCLUSION AND DISCUSSION

In the present paper, we proposed the bosonic $t-J$ model of hard-core atoms and studied its physical properties by means of the MC simulations. In Model II, the effects of the projection operator $P_x = 1 - \phi_x^\dagger \phi_x$ are ignored and, as a result, there appear four phases, AF, PM, PM+SF, and AF+SF phases. In Model I, we mostly studied the bond-breaking effects by holes and found that the AF+SF does not appear in the phase diagram. We also investigated if the PS takes place and found that, in both models, it does not.

We argued that Model II describes effectively a doped AF Heisenberg model including strong AF correlations besides the NN AF couplings, such as *the next-NN spin couplings*. Thus the important result of Model II, appearance of the AF+SF phase, suggests that such a coexisting phase of AF order and SF may be generated by inclusion of certain AF-enhancing couplings such as the next-NN coupling beyond the NN ones.

For the fermionic $t-J$ model, whether the AF+SF phase (or rather the coexisting phase of AF order and superconductivity) exists or not is an open question. However a AF+superconducting phase has been observed by recent experiments with uniform high-quality samples of high- T cuprates[25]. Therefore we expect that a similar coexisting phase of AF+SF appears in cold-atom systems in an optical lattice with strong on-site repulsion as long as certain AF-enhancing couplings such as next-NN coupling are involved.

Another interesting subject is to consider the effect of anisotropy of pseudo-spin coupling ($\alpha < 1$). Although we studied the isotropic case ($\alpha = 1$) in the present paper as the canonical case, the realistic cold-atom systems may have anisotropy. This is because the difference in two species of bosons such as their hopping amplitudes, etc., are reflected to this anisotropy in the resulting $t-J$ model (recall the relation $J = 4t^2/U$).

At the beginning of Sect.4, we mentioned the possible superconductivity via formation and condensation of NN hole pairs in Model I. Because we found no separated phase transition into superconducting phase in Sect.4, it is plausible that the superconducting state of hole pairs is generated simultaneously with the SF state of single-boson BEC. To examine this point further, it is necessary to study the correlation function of these pairs in details. When the anisotropy is included, such correlation may have different behaviors in different pairing chan-

nels. These topics (the next-NN coupling, anisotropy, and the hole-pairing) are under study. We hope to report on them in future publications.

Finally, studies on the bosonic $t-J$ model in the present and previous papers suggest for the fermionic $t-J$ model that, at finite hole concentrations, coherent holon hopping is realized. In the slave-fermion approach, this implies that a small Fermi surface of fermionic holons is generated in under-doped region. In the further study of the bosonic $t-J$ model, we expect to draw further interesting suggestions for the fermionic $t-J$ model and vice versa.

Acknowledgment

We thank Dr. Kenichi Kasamatsu for useful comments. This work was partially supported by Grant-in-Aid for Scientific Research from Japan Society for the Promotion of Science under Grant No.20540264.

Appendix A: CP¹ Representation of a Hard-core Boson

In this Appendix we derive the representation (1.3, 2.18) of a HCB operator in terms of a CP¹ spin operator $w_{x\eta}$.

Let us introduce an $s = 1/2$ SU(2) (pseudo) spin operator \vec{T}_x by using $w_{x\eta}$ as

$$\vec{T}_x = \frac{1}{2} \bar{w}_x \vec{\sigma} w_x, \quad (\text{A.1})$$

where $\vec{\sigma}$ are 2×2 Pauli matrices. Explicitly,

$$\begin{aligned} T_{x1} &= \frac{1}{2} (\bar{w}_{x1} x_{x2} + \bar{w}_{x2} x_{x1}), \\ T_{x2} &= -\frac{i}{2} (\bar{w}_{x1} x_{x2} - \bar{w}_{x2} x_{x1}), \\ T_{x3} &= \frac{1}{2} (\bar{w}_{x1} x_{x1} - \bar{w}_{x2} x_{x2}). \end{aligned} \quad (\text{A.2})$$

On the other hand, the rising operator T_x^+ and the lowering operator T_x^- defined by

$$T_x^\pm \equiv T_{1x} \pm iT_{2x}, \quad (\text{A.3})$$

is expressed by the HCB ϕ_x as

$$T_x^+ = \phi_x^\dagger, \quad T_x^- = \phi_x. \quad (\text{A.4})$$

Then we have

$$\phi_x = w_{x2}^\dagger w_{x1}, \quad (\text{A.5})$$

which is (1.3, 2.18). The correspondence between the two sets of states are as follows;

$$\begin{aligned} T_3|+\rangle &= \frac{1}{2}|+\rangle, \quad T_3|-\rangle = -\frac{1}{2}|-\rangle, \\ \phi|0\rangle &\equiv 0, \quad |-\rangle = |0\rangle, \quad |+\rangle = \phi^\dagger|0\rangle, \\ w_\eta|v\rangle &\equiv 0, \quad |-\rangle = w_2^\dagger|v\rangle, \quad |+\rangle = w_1^\dagger|v\rangle. \end{aligned} \quad (\text{A.6})$$

-
- [1] For experiments, see, e.g., M. Greiner, O. Mandel, T. Esslinger, T. Hänsch, and I. Bloch, *Nature* **415**, 39 (2002); F. Gerbier, S. Fölling, A. Widera, O. Mandel, and I. Bloch, *Phys. Rev. Lett.* **96**, 090401 (2006).
- [2] For theoretical study (of superfluid-Mott insulator transition), see, e.g., D. Jaksch, C. Bruder, J. I. Cirac, C. W. Gardiner, and P. Zoller, *Phys. Rev. Lett.* **81**, 3108 (1998).
- [3] K. Günter, T. Stöferle, H. Moritz, M. Köhl, and T. Esslinger, *Phys. Rev. Lett.* **96**, 180402 (2006); S. Ospelkaus et al., *Phys. Rev. Lett.* **96**, 180403 (2006).
- [4] J. Catani, L. De Sarlo, G. Barontini, F. Minardi, and M. Inguscio, *Phys. Rev. A* **77**, 011603(R) (2008).
- [5] G. Thalhammer, G. Barontini, L. De Sarlo, J. Catani, F. Minardi, and M. Inguscio, *Phys. Rev. Lett.* **100**, 210402 (2008).
- [6] M. Boninsegni, *Phys. Rev. Lett.* **87**, 087201 (2001); *Phys. Rev. B* **65**, 134403 (2002);
- [7] M.W. Long and X. Zotos, *Phys. Rev. B* **45**, 9932 (1992); L.-M. Duan, E. Demler, and M. D. Lukin, *Phys. Rev. Lett.* **91**, 090402 (2003).
- [8] M. Boninsegni and N.V. Prokof'ev, *Phys. Rev. B* **77**, 092502 (2008).
- [9] K. Aoki, K. Sakakibara, I. Ichinose, and T. Matsui, *Phys. Rev. B* **80**, 144510 (2009).
- [10] I. Ichinose and T. Matsui, *Phys. Rev. B* **45**, 9976 (1992); H. Yamamoto, G. Tataru, I. Ichinose, and T. Matsui, *Phys. Rev. B* **44**, 7654 (1991).
- [11] R. K. Kaul, M. A. Metlitski, S. Sachdev, and C. Xu, *Phys. Rev. B* **78**, 045110 (2008).
- [12] M. Boninsegni, *Phys. Rev. Lett.* **87**, 087201 (2001); *Phys. Rev. B* **65**, 134403 (2002).
- [13] We write the HCB operator as $B_{x\sigma}$ instead of $\hat{B}_{x\sigma}$ for simplicity.
- [14] The hard-core nature may be implemented by starting from the usual bosons without hard-core nature, adding to the Hamiltonian (2.1) the term $V \sum_{x\sigma} \hat{n}_{x\sigma} (\hat{n}_{x\sigma} - 1)$, and taking the limit $V \rightarrow \infty$. This term allows only for the states $\hat{n}_{x\sigma} = 0, 1$ and excludes the states $\hat{n}_{x\sigma} > 1$.
- [15] $[A, B]_+ \equiv AB + BA$ is the anticommutation relation.
- [16] There appears another term $\sum_x \sum_{\mu, \nu} \epsilon_{\sigma\sigma'} B_{x\sigma}^\dagger B_{x+\mu, \sigma'} \times \epsilon_{\tau\tau'} B_{x+\mu, \tau}^\dagger B_{x+\nu, \tau'}$. However, their coefficient has an extra factor $\propto \delta$ and can be negligible for small hole concentrations.
- [17] This restriction to the physical space is exactly the same as in the fermionic t - J model.
- [18] See, e.g., P. A. Lee, N. Nagaosa, and X-G Wen, *Rev. Mod. Phys.* **78**, 17 (2006).
- [19] See I. Ichinose, T. Matsui, and M. Onoda, *Phys. Rev. B* **64**, 104516 (2001) and the references cited therein.
- [20] For general s , the constraint (2.11) becomes $(2s)^{-1} \sum_{\sigma=1}^2 a_{x\sigma}^\dagger a_{x\sigma} + \phi_x^\dagger \phi_x = 1$. There are $2s + 1$ possible physical states for each x . For example, the states for $s = 1$ are described by $(z_{x\uparrow}^\dagger z_{x\uparrow}^\dagger, z_{x\uparrow}^\dagger z_{x\downarrow}^\dagger, z_{x\downarrow}^\dagger z_{x\downarrow}^\dagger) |0\rangle$.
- [21] Again we used the same letter $B_{x\sigma}$ as the operator (2.2) because no confusions arise.
- [22] As we are considering a quantum system, a state at each site is generally given by a superposition of the holon state and the spinon state. The quantum state that is totally occupied by a holon is a very specific state.
- [23] The experimental relevance of the phase diagram in the δ - T plane of the fermionic t - J model is discussed in A. Eckardt and M. Lewenstein, arXiv: 1001.1918.
- [24] For the 2D system, the number of broken AF bonds are seven for a NN holon pairs and eight for a more separated pair.
- [25] H. Mukuda, M. Abe, Y. Araki, Y. Kitaoka, K. Tokiwa, T. Watanabe, A. Iyo, H. Kito, and Y. Tanaka, *Phys. Rev. Lett.* **96**, 087001 (2006).